International Journal of Thin Films Science and Technology

http://dx.doi.org/10.18576/ijtfst/080310

Effects on the linear and nonlinear optical properties of Se-S-Sb chalcogenide glass thin films

E. R. Shaaban[1,], M. M. Soraya[2], M. M. Samar[2] and El Sayed Yousef[3,4]*

[1] Physics Department, Faculty of Science, Al-Azhar University, Assuit, 71542, Egypt,
[2] Department of Physics, Faculty of Science, Aswan University, Egypt,
[3] Physics Department, Faculty of Science, King Khalid University, P.O. Box 9004, Abha, Saudi Arabia,
[4] Research Center for Advanced Materials Science (RCAMS), King Khalid University, Abha 61413, P.O. Box 9004, Saudi Arabia.

Received: 3 Mar. 2019, Revised: 3 Jun. 2019, Accepted: 17 Jul. 2019

Published online: 1 Sep. 2019

Abstract: Different composition of $Se_{80-x}S_{20}Sb_x$ (x=0, 2.5, 5, 7.5, 10) thin film were prepared by thermal evaporation techniques at room temperature. The amorphous crystalline nature of the investigated films was confirmed by X-ray Diffraction technique. Optical properties were calculated over a wide wavelength (500–2500 nm) using spectrophotometric measurements of transmittance and reflectance. The optical constants (n, k) for thickness (d) of the samples were analysis from optical transmittance data using the Swanepoel method. It was found that refractive index increases with increasing Sb content in $Se_{80-x}S_{20}Sb_x$ thin films while the optical band gap energy decreases as the Sb content increases. In terms of the Wemple–DiDomenico single-oscillator model the dispersion of the refractive index is calculated from the result of refractive index. The oscillator parameters such as the single-oscillator energy E_o, the dispersion energy E_d, the static refractive index n (0), high frequency dielectric constant **(ε_∞)**, the optical and the electrical conductivities have been estimated and it found to be Sb content dependent. From the values of the dielectric constants, the energy loss factor and energy loss functions have been analyzed. Also, the nonlinear refractive index has been investigated according to Tichy-Ticha and Fournier- Snitzer models.

Keywords: *$Se_{80-x}S_{20}Sb_x$; Swanepoel method; optical constants; Energy loss functions; nonlinear refractive index.*

1 Introduction

Chalcogenide glasses are inorganic glass materials which containing Sulphur, selenium and tellurium of the main group III–V elements. They have amorphous semiconductor nature as they possess energy band gap ranging from 1 to 3 eV. These materials have excellent infrared applications since IR transmission has very wide range from 0.5 to 16 µm [1, 2]. These glasses have many useful applications in various fields as in optical switching, fibers, optical imaging, laser power delivery, chemical sensing, imaging scanning near field microscopy/spectroscopy, IR sources/lasers, realization of microstructures in integrated optics and amplifiers [3–5]. Chalcogenide elements have good abilities to obtained in amorphous thin film phase preparing by variety methods such as oregano-metallic chemical vapor deposition, thermal evaporation under vacuum, molecular beam epitaxy (MBE), solution growth spray pyrolysis and other techniques [6,7]. One of the chalcogenide compounds Sb_2S_3 and Sb_2Se_3 are important photoconductive semiconductors (Eg with 1.64 and 1.11 eV, respectively) with orthorhombic crystal structure [8]. Now days Sb_2Se_3has attention in different potential application in PC RAM [9], thermoelectric devices [10], photodetectors [11], photovoltaics [12] because of its good optical and electrical properties. On the other hand, Sb_2S_3 plays important role with its applications as a sensitive material for television cameras, as well as in microwave, switching, and optoelectronic devices [13-15]. Continually, in order to obtain amorphous (Se-S-Sb) thin film a solid solution occur among them (Sb_2S_3 and Sb_2Se_3) to achieve anew alloy with specific characteristics and keeping the advantages of both Sb_2S_3 and Sb_2Se_3.Many investigations carried out the composition $Sb_2Se_{3-x}S_x$ which confirms that it has photoelectric properties since it has tunable band gap so that it plays important role in solar cell application [16-18]. Also, the effect of compositional variations on the optical properties of Sb_xSe_{60-x} S_{40} thin films has been studied by Ramakanta Naik and R. Ganesan [19].

*Corresponding author E-mail: esam_ramadan2008@yahoo.com

In the present search, the compositional $Se_{80-x}S_{20}Sb_x$ thin film prepared by thermal evaporation technique. Different techniques have been used to study the structure parameters of chalcogenide glasses, such as X-ray diffraction studied to show nature and phase of thin films. The optical properties of different compositions of (Se-S-Sb) system illustrated in term of spectroscopic measurements, therefore the refractive index, extinction coefficient and other optical constants of the films have been investigated. Also, nonlinear optical properties have been studied.

2 Experimental procedures

Various composition of chalcogenide glass $Se_{80-x}S_{20}Sb_x$ (x = 0, 2.5, 5, 7.5, 10) in the form of bulk is prepared by using the typical melt quenching technique. The material of Se, S and Sb were prepared from the high purity (99.999% pure). Then appropriate volume of component weighed according to their atomic percentages to be ready to charge into clean silica quartz ampoules after that they sealed under the vacuum of pressure about10^{-4} Pa. In order to achieve a homogenous structure of amorphous solid the silica ampoule put inside a rotated furnace and heated slowly to 950 °C with a temperature gradient about of 5^0 C/min and the ampoule kept rotating until 24 h this is known as melting process. After homogenization of the melt completed the ampoules quenched quickly in ice water to avoid crystallization of materials.

Different bulk composition of $Se_{80-x}S_{20}Sb_x$ were prepared as thin film in glass substrate by the mean of electron-beam evaporation technique using a high vacuum coating unite(Edwards type E 306 A England).The films were deposited on glass and fused silica substrates of size 25 mm x 25 mm x 2.5 mm at pressure equal to 1 x10 $^{-6}$ Pa. Through the deposition process the substrates were reserved at room temperature 300 K and the rate of deposition was kept constant during evaporation process just about 2 nm/s. In order to achieve homogenous and smooth films, the substrates were rotated slowly at speed of 3 rev/min. Also, through the evaporation treatment the thickness of the formed films was monitored by using quartz crystal thickness monitor (Model FTM4, Edwards Co., England). The structure nature of amorphous films was checked by using advanced computerized diffractometer type (Philips XPert) provided by a nickel-filtered Cu-Kα radiation. The essential composition of deposited films was determined by using an energy-dispersive X-ray spectrometer (EDXS) unite. Moreover, the morphology of thin films was analyzed in term of electron microscope, SEM (JOEL XL) operating at an accelerating voltage of 30 KV. The optical parameter such as transmittance T and reflectance R were determined by using UV-VIS-NIR JASCO-670 double-beam spectrophotometer in the spectral range 400-2500 nm at room temperature. At normal incidence the transmittance spectra were measured with unpolarized light deprived of a substrate in the reference beam, while the reflectance spectra calculated by using reflection attachment nearly to normal incidence (~ 5^0).

3. Results and discussion

3.1 XRD analysis

XRD patterns of $Se_{80-x}S_{20}Sb_x$ (x = 0, 2.5, 5, 7.5, 10) chalcogenide glass thin films with the thickness (d =725 nm approximately) deposited at ambient temperature are shown in Fig.1. The X-ray intensity data were collected in the angular ranges 2θ = 4-90°. The absence of any sharp peaks emphasizes the glassy nature of these compositions. For further clarification of the patterns, these amorphous samples had approximately a broad hump of all the samples, which seems to act as two broadening humps overlaps together, their features were overshadowed. That may illustrate the single phase of these amorphous structures.

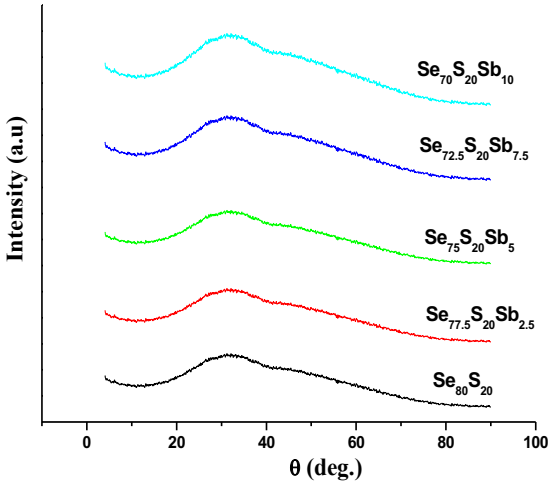

Fig (1) X-ray diffraction patterns for different composition of amorphous $Se_{80-x}S_{20}Sb_x$ (x=0,2.5,5,7.5,10) thin films.

3.2 Optical Characterization

3.2.1 Transmittance and reflectance spectral distribution

Fig.2 shows the transmittance, T and reflectance, R spectra of the deposited $Se_{80-x}S_{20}Sb_x$ (x = 0, 2.5, 5, 7.5, 10) chalcogenide glass thin films as a function of wavelength. The fundamental absorption moves towards the longer wavelength as Sb contents increases in the Se-S glassy alloys. This is considered as a result of shrinking the energy gap as Sb exchange for Se atoms in the Se-S glass.

3.2.2 The refractive index and film thickness

Fig.3 (a-e) shows the interference fringes and the created upper and lower envelopes for each specimen. The figure shows obviously two different regions, the strong absorption region and the medium-weak one. In the spectral region of weak and medium absorption, the first,

approximate value of the refractive index of the film n1, can be estimated, using Swanepoel calculations based on Manifacier et al idea [20] according to the relation:

$$n = \left[N + \left(N^2 - s^2\right)^{1/2}\right]^{1/2} \quad (1)$$

Where

$$N = 2s\,\frac{T_M - T_m}{T_M T_m} + \frac{s^2 + 1}{2}$$

Here T_M and T_m, are the transmission maximum and the corresponding minimum at a certain wavelength. The needful values of the refractive index of the substrate s are attained from the transmission spectrum of the substrate, Ts using the expression [21].

$$s = \frac{1}{T_s} + \left(\frac{1}{T_s} - 1\right)^{\frac{1}{2}} \quad (2)$$

The values of the refractive index n, as calculated from Eq. (1) are shown in table (1. a-e). Now, it is indispensable to take into consideration the main equation for interference fringes

$$2nd = m\lambda \quad (3)$$

where the order numbers m is integer for maxima and half integer for minima. Furthermore, if n_{e1} and n_{e2} are the refractive indices at two adjacent maxima (or minima) at λ_1 and λ_2, it follows that the film thickness is given by the relation:

$$d = \frac{\lambda_1 \lambda_2}{2\left(\lambda_1 n_{e2} - \lambda_2 n_{e1}\right)} \quad (4)$$

The values of d of different samples thickness determined by this equation are listed as d1 in table (1 a-e). The average value of d1, can now be used, along with n1, to calculate the "order number" m0 for the different extremes using Eq.3. The accuracy of d can now be significantly increased by taking the corresponding exact integer or half integer values of m associated to each extreme and deriving a new thickness, d2 from Eq. (3), again using the values of n1, The values of d found in this way have a smaller dispersion ($\sigma 1 > \sigma 2$). The final values of the refractive index n2 are obtained as shown in table (1 a-e).

Fig.4 shows the dependence of n on wavelength for different glassy compositions of $Se_{80-x}S_{20}Sb_x$ (x = 0, 2.5, 5, 7.5, 10) chalcogenide glass thin films. According to the dispersion function such as the two-term Cauchy function, $n(\lambda) = B + A/\lambda^2$,the values of n can be fitted, which can be used for extrapolation the whole wavelength dependence of refractive index, as shown by Fig.4.The value of Cauchy parameters, A and B are listed in table (2). Fig.4 shows that the refractive index increases with increasing Sb content, over the entire spectral range studied. This increase is related to the increased polarizability of the Sb atoms due to the larger atomic radius (1.53 A°), in comparison with the smaller one of the Se atoms (1.22 A°).

3.2.3 The high- frequency dispersion parameters

According to the single-oscillator model (Wemple and DiDomenico dispersion relationship) [22], the energy dependence of n of amorphous materials can be fitted, where E_0 is the single-oscillator energy and E_d is the dispersion energy.

$$n^2 - 1 = \frac{E_o E_d}{E_o^2 - (h\nu)^2} \quad (5)$$

By plotting $(n^2 - 1)^{-1}$ versus *hv* and filling the data to a straight line (as shown in Fig.5, E_0 and E_d can be determined from the slope, −1/E0Edand the intercept, E_0/E_d. The values obtained for dispersion parameters Ed and E_0 for five thin films samples are listed in table (3). Fig.5 also shows the values of the refractive index n (0) at *hv = 0* for the $Se_{80-x}S_{20}Sb_x$ (x = 0, 2.5, 5, 7.5, 10) thin films. The obtained values of *n (0)* are listed in table (3). It was noticed that, with increasing Sb content the single-oscillator energy decreases while the dispersion energy and the static refractive index *n (0)* increase. The oscillator energy, E_o, is the average energy gap parameter and with a good approximation it varies in proportion to optical band gap ($E_o \approx 2Eg$) [23]. The dispersion energy or single-oscillator strength, E_d, considered as a measure of the strength of interband transitions [24]. E_d increases with increasing Sb content, while there is a decrease in the Se-Se homopolar bonds as shown in table (4). It means antimony is more coordinated in the glass matrix.

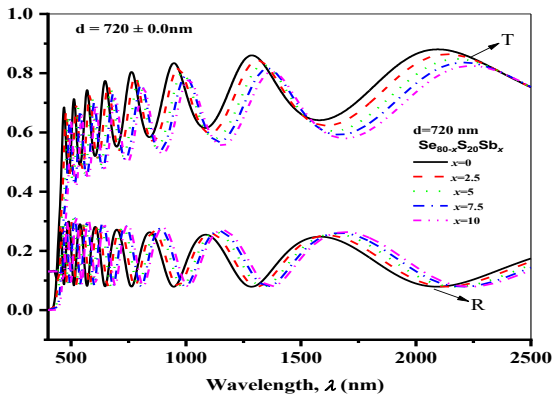

Fig (2) A typical optical transmission–reflection spectra for different composition of amorphous $Se_{80-x}S_{20}Sb_x$ (x=0,2.5,5,7.5,10) thin films.

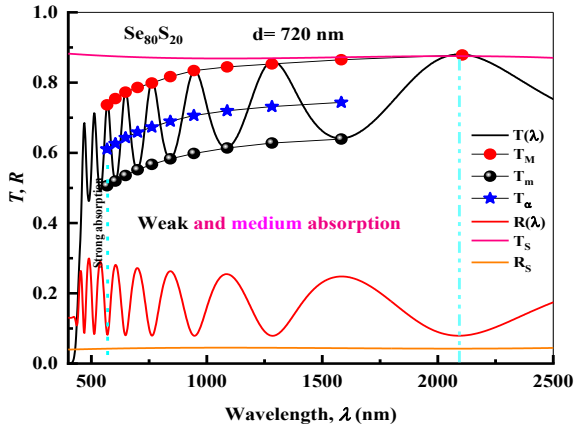

Fig (3a) A typical optical transmission–reflection spectra versus wavelength λ for amorphous $Se_{80}S_{20}$ thin films.

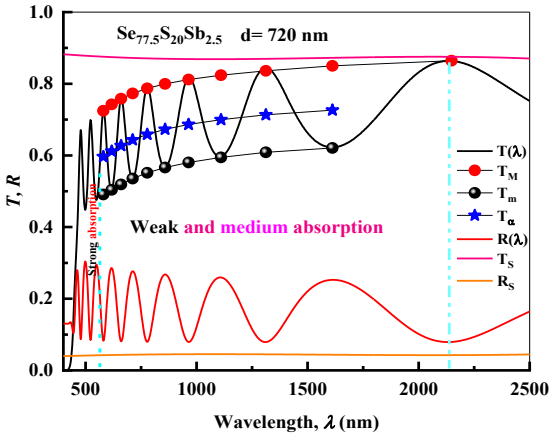

Fig (3b) A typical optical transmission–reflection spectra versus wavelength λ for amorphous $Se_{77.5}S_{20}Sb_{2.5}$ thin films.

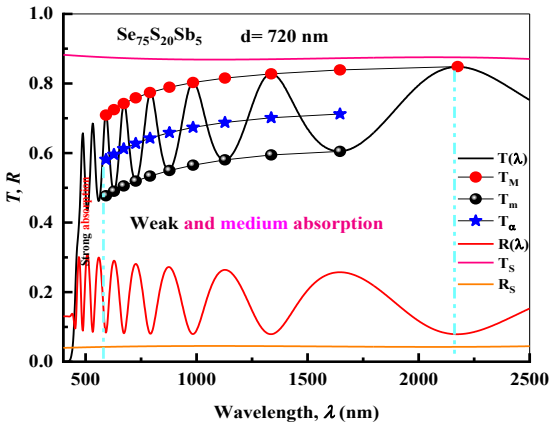

Fig (3c) A typical optical transmission–reflection spectra versus wavelength λ for amorphous $Se_{75}S_{20}Sb_5$ thin films.

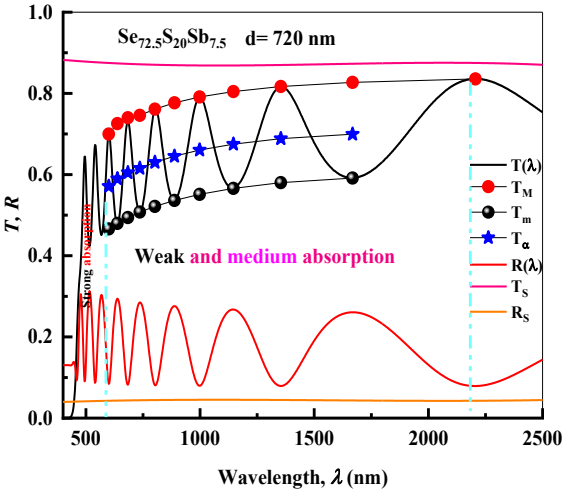

Fig (3d) A typical optical transmission–reflection spectra versus wavelength λ for amorphous $Se_{72.5}S_{20}Sb_{7.5}$ thin films.

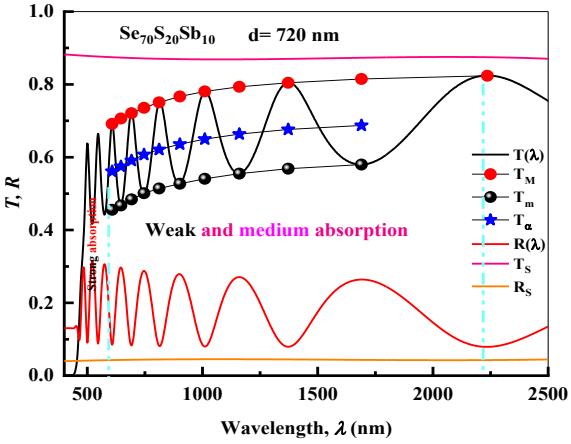

Fig (3e) A typical optical transmission–reflection spectra versus wavelength λ for amorphous $Se_{70}S_{20}Sb_{10}$ thin films.

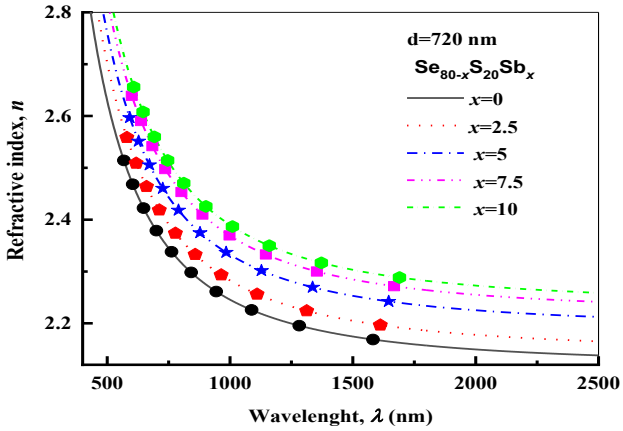

Fig (4) Spectral distribution of refractive index n, versus wavelength λ for different composition of amorphous $Se_{80-x}S_{20}Sb_x$ (x=0,2.5,5,7.5,10) thin films.

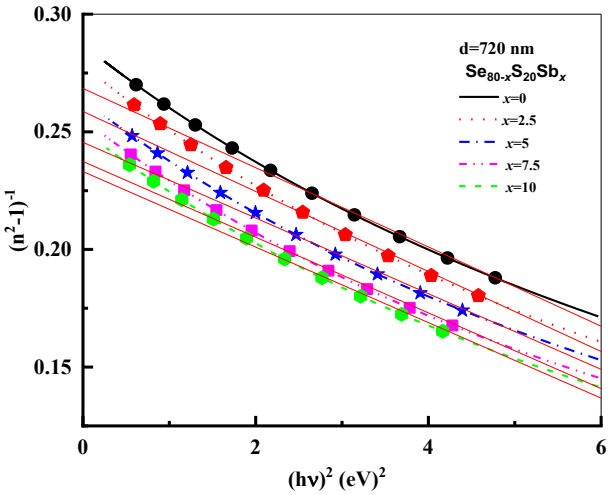

Fig (5) Plot of refractive index factor $(n^2 - 1)^{-1}$ versus (hv)2 for different composition of amorphous $Se_{80-x}S_{20}Sb_x$ (x=0,2.5,5,7.5,10) thin films.

3.2.4 The high frequency dielectric constant (ε∞) and the ratio of (N/m)*

The achieved data of refractive index can be used to analyze the high-frequency dielectric constant describing the contribution of the free carriers and lattice vibration modes of the dispersion, the real component of the relative permittivity (ε) and square of wavelength (λ^2) are related by [25].

$$\varepsilon = n^2 = \varepsilon_\infty - \left(e^2 / 4\pi^2 \varepsilon_\circ c^2\right)\left(N/m^*\right) \lambda^2 \qquad (6)$$

Where n is the refractive index, e is the electron charge and c is the velocity of light, ε_∞ is the lattice dielectric constant, ε_0 is the free space permittivity. By blotting n^2 versus λ^2 as shown in Fig.6, the values of ε∞ and the ratio (N/m*) are analyzed then summarized in table. 3. It is obviously that the increasing of Sb within the specimens increase the values of ε∞ and the ratio (N/m*).

3.2.5 The absorption, extinction coefficients and optical band gap

The optical transmittance (T) and the reflectance (R) spectral dependence of the samples under investigation can be achieved using a double-beam spectrophotometer. The absorption coefficient α can be obtained in the strong absorption region of the experimentally measured values of R and T in accordance with the subsequent relation [26]:

$$\alpha = \frac{1}{d} \ln\left[\frac{(1-R)^2 + \left[(1-R)^4 + 4R^2T^2\right]^{1/2}}{2T}\right] \qquad (7)$$

where d is the film thickness. The absorption coefficient as a function of photon energy for the different compositions of Se_{80-x}-S_{20}-Sb_x (x = 0, 2.5, 5, 7.5, 10) chalcogenide glass thin films is illustrated in Fig.7, the figure illustrate three different regions, Tauc region in which the band gab can be estimated, the Urbach tail in which the absorption is due to the localized state within the band gab and weak absorption region. It is clear that the absorption edge ($\alpha \geq 10^4$) shifts towards the less photon energy with increasing Sb contents in all the specimens under study due to decreasing of optical band gap as a result of Sb additive.

It is available now to calculate the extinction coefficient from the values of λ and α using the expression $k = \alpha\lambda/4\pi$. Fig.8 illustrates the dependence of k on the wavelength for different thin films of $Se_{80-x}S_{20}Sb_x$ (x = 0, 2.5, 5, 7.5, 10) glasses. It should be pointed out that the absorption coefficient of amorphous semiconductors, in the high-absorption region ($\alpha \geq 10^4$), is given by Tauc's relation for the allowed non-direct transition [27] by the subsequent formula:

$$\alpha h\nu = A(h\nu - E_g^{opt})^2 \qquad (8)$$

where A is a constant which depends on the transition probability and E_g^{opt} is the optical band gap. Fig.9 shows a good fitting of $(\alpha h\nu)^{1/2}$ versus photon energy ($h\nu$) for five different compositions of thin films. The values of the optical band gap E_g^{opt} were taken as the intercept of $(\alpha h\nu)^{1/2}$ versus ($h\nu$)at $(\alpha h\nu)^{1/2} = 0$ in accordance with Tauc's allowed non-direct transition. The optical band gap derived for each film is listed in table (3).

Urbach energy

At lower values of the absorption coefficient ($1 \leq \alpha \leq 104 cm^{-1}$), the absorption depends exponentially on the photon energy (the so-called Urbach relation [28])

$$\alpha(h\upsilon) = \alpha_0 \exp\left(\frac{h\upsilon}{E_e}\right) \qquad (9)$$

where α0 is a constant and Ee is the Urbach energy (the band tail width of the localized states at the valence band edge). Fig.10 shows the dependence of ln(α) on photon energy hv for the different compositions of amorphous Se80-xS20Sbx (x = 0, 2.5, 5, 7.5, 10) films. The values of the Urbach energy, Ee for the five different thin films are analyzed and listed in table (3). It is significant that Energy gap E_g^{opt} decreases with increasing Sb content but the Urbach energy Ee increase, this mean that an additional of Sb lead to an increase of the localized states within the band gap. Davis and Mott [29] reported that the presence of high density of localized state in the band structure is responsible for shrinkage of optical gap.

3.2.6 Determination of the dielectric constants and loss factor

It is common that the complex dielectric constant $\tilde{\varepsilon}$ is mainly consist of two important parts that is, $\tilde{\varepsilon} = \varepsilon_r + i\,\varepsilon_i$

where, ε_r is the real part of the dielectric constant, $\varepsilon_r = n^2 - k^2$, it indicates how much will weaken the light velocity in the material, whereas the imaginary part, $\varepsilon_i = 2nk$ indicates how much the electrical energy absorbed by the dielectric materials due to dipole motion [30]. Fig.11 and Fig.12 show the variations of the real and imaginary dielectric constant parameters respectively with wavelength. It was clear that the real part, ε_r and imaginary part, ε_i of the dielectric constant decreases with wavelength in all specimens and increases with increasing Sb content within the samples under investigation, also it was obviously from the last two figures that the values of ε_r are higher than that of ε_i for all samples.

It is convenient now to calculate the tangent or loss factor (dissipation factor), which depend directly on the real and imaginary parts of the dielectric constant throw the following relation [31]:

$$\tan(\delta) = \frac{\varepsilon_i}{\varepsilon_r} \tag{10}$$

Fig.13 plots the variations of loss factor as a function of photon energy. This figure indicates that the dissipation factor increases with increasing Sb content within the samples and with increasing the photon energy in all specimens.

Energy loss function

The term ELF refers to the energy loss function which can be classified to surface energy loss function, SELF and volume energy loss function. This classification depends on the free carriers transitions through material, if they lose their absorption of light energy at the surface (SELF) or out of the volume (bulk) of material (VELF). The surface energy loss function, SELF and volume energy loss function, VELF can be calculated as [32, 33]:

$$SELF = \frac{\varepsilon_i}{((\varepsilon_r^2 + 1) + \varepsilon_i^2)} \tag{11}$$

$$VELF = \frac{\varepsilon_i}{(\varepsilon_r^2 + \varepsilon_i^2)} \tag{12}$$

Fig.14 shows SELF and VELF functions variations with photon energy, it is easy to notice that the two functions increase with increasing photon energy for all specimens and with increasing Sb contents.

3.2.7 Determination of the optical and electrical conductivities

Optical conductivity, σ_{opt} is one of the significant tools for studying the electronic states in materials and can be obtained via the absorption coefficient, α and refractive index, n [34]:

$$\sigma_{opt.} = \alpha n c \varepsilon_0 = \frac{\alpha n c}{4\pi} \tag{13}$$

Where c is the light velocity and $\varepsilon_0$the electrical permittivity of the space and equal to (8.854×10^{-12} F/m).Fig.15 plots the variation of optical conductivity, σ_{opt} as a function of photon energy, $h\nu$. The optical conductivity increases exponentially with increasing photon energy, also increase with increasing Sb contents within the samples. The increase of optical conductivity at high photon energies may be due to the high absorbance of thin films [35].

Also, the electrical conductivity can now be obtained according to the relation

$$\sigma_e = \frac{2\lambda\sigma_{opt.}}{\alpha} \tag{14}$$

Fig.16 shows the variation of electrical conductivity σ_e with photon energy, that results clarify a decrease of electrical conductivity with photon energy while it increases with increasing Sb contents within samples as an expected result of decreasing the energy gab as we mentioned above.

3.2.8 Determination of non-linear refractive index

To determine the nonlinear refractive index , n_2 according to Tichy and Ticha relationship [36]. It should be at first determine $S^{(3)}$ the third order non-linear susceptibility which computed from the following relation[37]

$$S^{(3)} = A[S^{(1)}]^4 \tag{15}$$

$$S^{(3)} = \frac{A}{(4\pi)^4}\left(n_o^2 - 1\right)^4 \tag{16}$$

Where A = 1.7×10^{-10} (for $S^{(3)}$ in esu).

Tichy and Ticha relationship is a combination of Miller's popularized rule and static refractive index computed from WDD model as [36,38]:

$$n_2 = [\frac{12\pi}{n_o}]S^{(3)} \tag{17}$$

Fig.17 plots the non-linear refractive index according to Tichy and Ticha relationship versus wavelength. It is obviously that the non-linear refractive index decreases with increasing the wavelength and increase with increasing Antimony contents within samples.

Fournier and Snitzer [39] proposed another way to determine the non-linear refractive index which based on

linear refractive index (n) and WDD parameters (Eo, Ed) in the subsequent formula:

$$n_2 = \frac{(n^2+2)^2(n^2-1)}{48\pi nN}[\frac{E_d}{E_o^2}] \quad (18)$$

where N is the density of polarizable constituents which is computed using density/molar volume data. The nonlinear refractive index is deduced in esu [40,41].

The molar volume given by Eq. (20) was obtained:

$$V_m = \frac{1}{\rho}\sum_j \Gamma_j M_j \quad (19)$$

Where M_j is the molecular weight of the j[th] component, Γ_j is the atomic percentage of the same element in the film and ρ is the density of the system.

The density of the system is computed theoretically using the following relation:

$$\rho = \frac{\alpha\rho_{Se} + \beta\rho_S + \gamma\rho_{Sb}}{\alpha+\beta+\gamma} \quad (20)$$

Where α, β, γ are the ratios of the elements $(\alpha+\beta+\gamma=100)$.

Fig.18 shows the variation in nonlinear refractive index, n_2 according to Fournier and Snitzer relationship with wavelength. It is clear from Fig. 18 that nonlinear refractive index, n_2 increase with increasing Sb contents within samples while, decrease with increasing wavelength, the same trend as the nonlinear refractive index deduced by Tichy and Ticha.

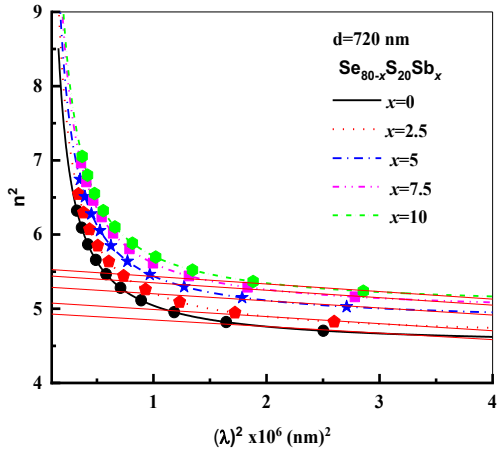

Fig (6) Shows the plots of n^2 versus λ^2 for different composition of amorphous $Se_{80-x}S_{20}Sb_x$ (x=0,2.5,5,7.5,10) thin films.

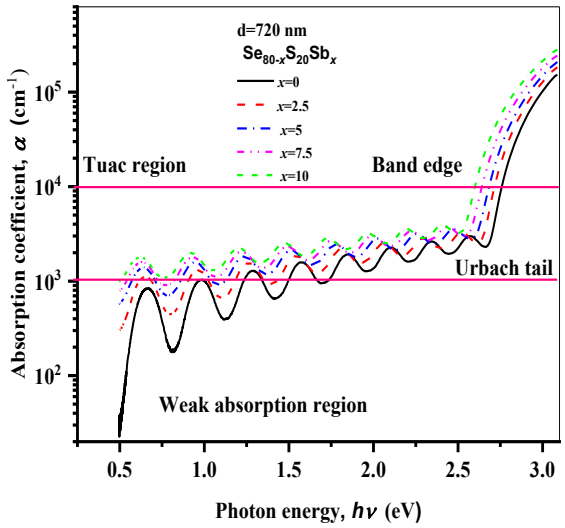

Fig (7) Shows the dependence of Absorption coefficient (α) on the incident photon energy (hv) for different composition of amorphous $Se_{80-x}S_{20}Sb_x$ (x=0,2.5,5,7.5,10) thin films.

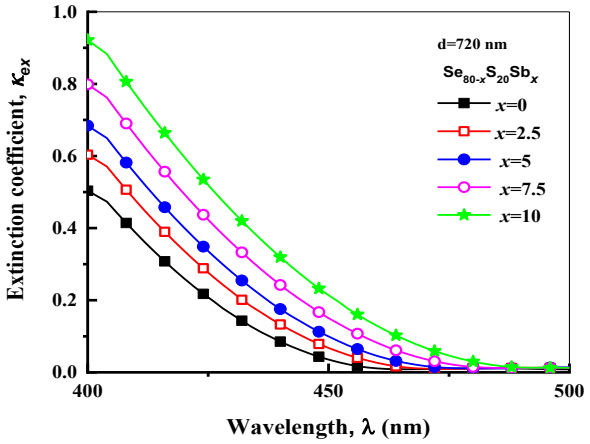

Fig (8) Shows the dependence of Extinction coefficient (k) on the wavelength (λ) for different composition of amorphous $Se_{80-x}S_{20}Sb_x$ (x=0,2.5,5,7.5,10) thin films.

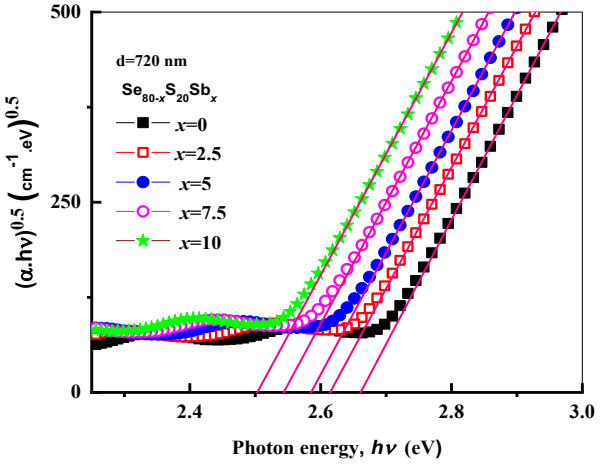

Fig (9) The dependence of $(\alpha h\nu)^{1/2}$ on photon energy (hv) for different composition of amorphous $Se_{80-x}S_{20}Sb_x$ (x=0,2.5,5,7.5,10) thin films, from which the optical band gap is estimated (Tauc's extrapolation).

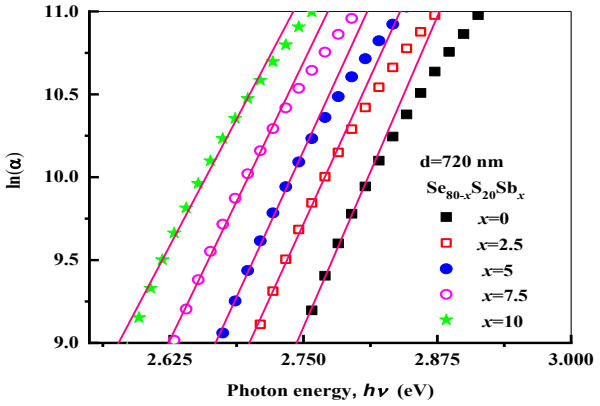

Fig (10) The dependence of ln(α) on photon energy (hv) for different composition of amorphous $Se_{80-x}S_{20}Sb_x$ (x=0,2.5,5,7.5,10) thin films, from which the Urbach energy Ee is estimated.

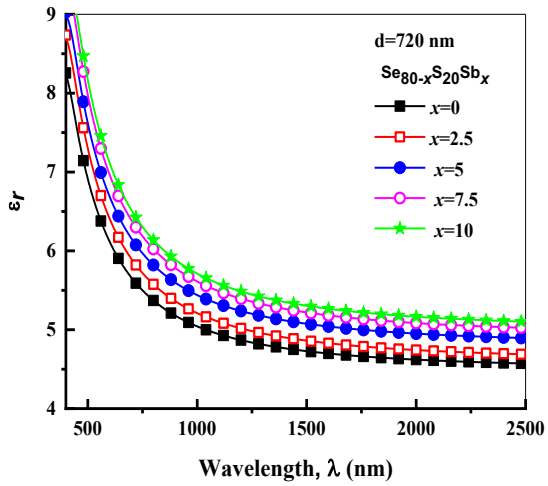

Fig (11) The real part (ε_r) of the dielectric constant as a function of wavelength for different composition of amorphous $Se_{80-x}S_{20}Sb_x$ (x=0,2.5,5,7.5,10) thin films.

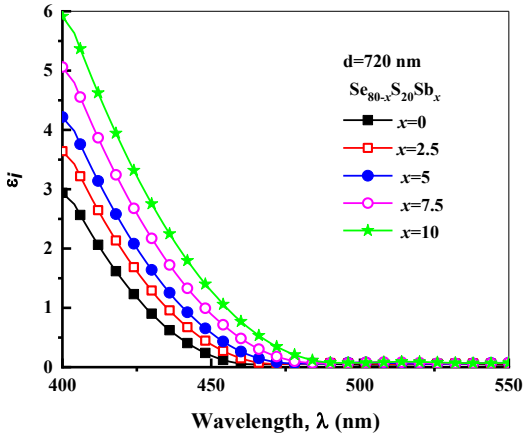

Fig (12) The imaginary part (εi) of the dielectric constant as a function of wavelength for different composition of amorphous $Se_{80-x}S_{20}Sb_x$ (x=0,2.5,5,7.5,10) thin films.

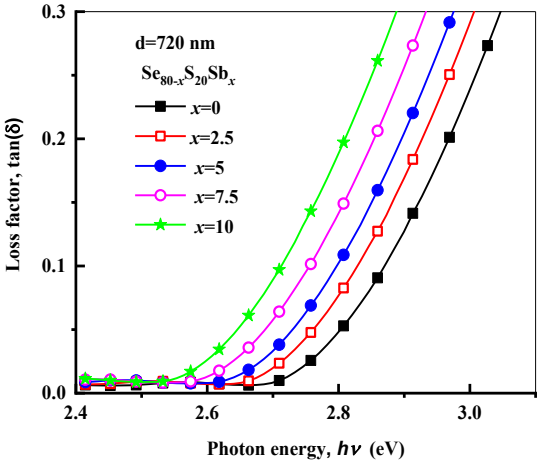

Fig (13) plots the variations of loss factor as a function of photon energy for different composition of amorphous $Se_{80-x}S_{20}Sb_x$ (x=0,2.5,5,7.5,10) thin films.

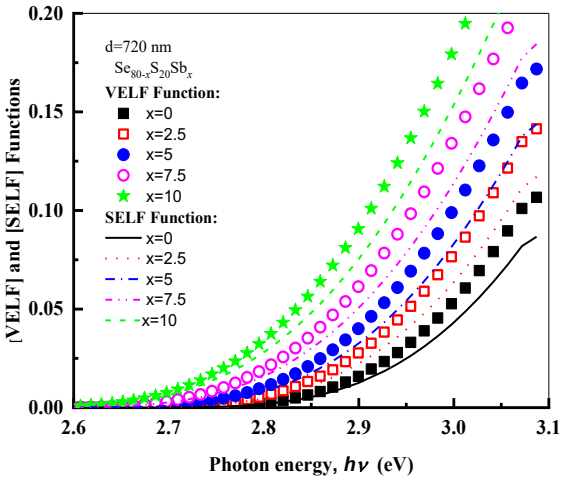

Fig (14) shows the graphical representation of the spectral variation of the volume (VELV) and surface (SELV) energy loss functions as a function of the photon energy for different composition of amorphous $Se_{80-x}S_{20}Sb_x$ (x=0,2.5,5,7.5,10) thin films.

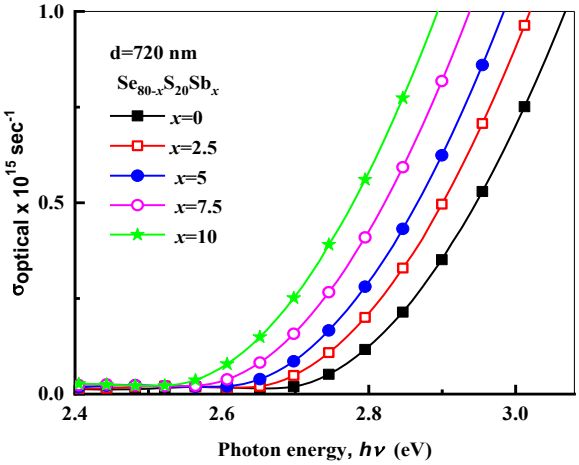

Fig (15) plots the variation of optical conductivity (σopt) as a function of photon energy (hv) for different composition of amorphous $Se_{80-x}S_{20}Sb_x$ (x=0,2.5,5,7.5,10) thin films.

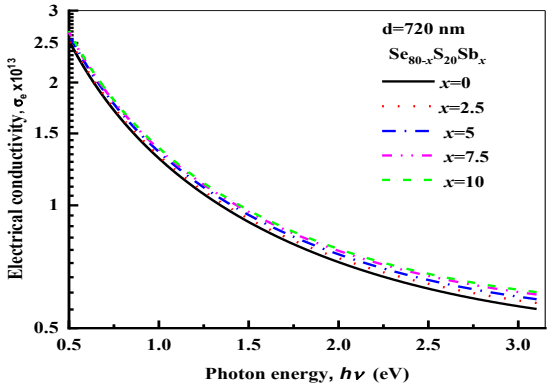

Fig (16) plots the variation of electrical conductivity(σe) as a function of photon energy (hv) for different composition of amorphous $Se_{80-x}S_{20}Sb_x$ (x=0,2.5,5,7.5,10) thin films.

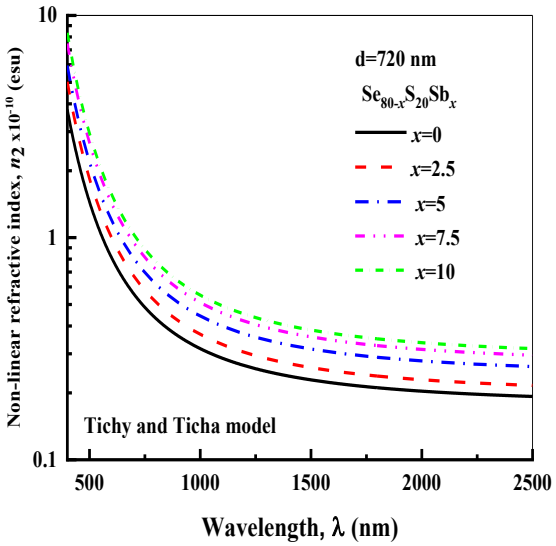

Fig (17) plots the non-linear refractive index according to Tichy and Ticha relationship versus wavelength for different composition of amorphous $Se_{80-x}S_{20}Sb_x$ (x=0,2.5,5,7.5,10) thin films.

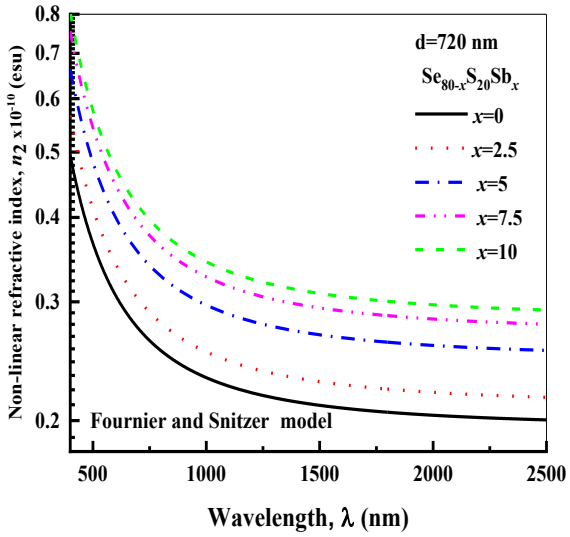

Fig (18) plots the non-linear refractive index according to Fournier and Snitzer relationship versus wavelength for different composition of amorphous $Se_{80-x}S_{20}Sb_x$ (x=0,2.5,5,7.5,10) thin films.

3.3 The theoretically calculated structural criterions:

The average coordination number, Nc

It is well known that the coordination number, the bonding character in the nearest-neighbor region describes the electronic properties of the semiconductors. It obeys the so-called 8-N rule, where N is the valency of an atom [42]. In accordance with this rule, the coordination number for Se, S, and Sb are listed in table (4), the average coordination

number, CN, of Sex-Sy-Sbz ternary composition can be defined as [43]:

$$\mathrm{CN} = (xCn(Se) + yCn(Te) + zCn(Sb)) \quad (21)$$

x, y, z are the ratios of these elements in the chalcogenide glass system, ($x + y + z = 1$). The calculated values of ***CN*** of Se_{80-x}-S_{20}-Sb_x (x = 0, 2.5, 5, 7.5, 10) are listed in table (5). It can be seen that coordination number increases with increasing the Sb content (as a result of Sb additive to Se-S matrix).

The numbers of lone pairs electrons

The numbers of lone pairs associated with the studied compositions were analyzed according to the equation [44]:

$$L = V - CN \quad (22)$$

where L and V are lone-pair electrons and valence electrons, respectively. The calculated values of lone pair electrons are given in table (5). It is obviously that the number of lone pairs electrons decreases with increasing Sb content within the composition.

The bond energies:

In order to investigate the structure and properties of numerous types of amorphous chalcogenide, in accordance with the chemical bond approach, atoms combine more favorably with atoms of different kinds than with the same kind; this assumption which is generally found to be valid for glass structures, has been used by Zachariasen [45] in his covalently bonded continuous random network model. According to this supposition, bonds between identical atoms will only take place if there is an excess of a certain type of atoms. Bonds are formed in the sequence of decreasing bond energies until all available valences for the atoms are saturated. The bond energies D(A–B) for heteronuclear bonds have been calculated by using the relation [42]

$$D(A-B) = \left[D(A-A) \times D(B-B)\right]^{1/2} + 30(\chi_A - \chi_B)^2 \quad (23)$$

where D(A–A) and D(B–B) are the energies of the homonuclear bonds, xA and xB are electronegativity values for atoms involved. Both the electronegativity and the homonuclear bonds D (A–A) and D(B–B) for S, Se and Sb are listed in table (4). The types of bonds expected to occur in the investigated system are Se-S bonds (52.843 kcal/ mol), S-Sb (52.178 kcal/mol), Se–Sb (43.981 kcal/mol) and Se-Se bonds (44.04 kcal/ mol). In the present glassy compositions, the Se atoms strongly bond to S. The Se-S bonds have the highest probability to exist, then the S-Sb bonds and finally the Se–Sb bonds. After these bonds are formed, there are still unsatisfied Se valences, which are much satisfied by the formation of Se–Se bond.

The cohesive energy (*CE*)

Knowing the bond energies, the cohesive energy (*CE*) have been achieved by assuming the bond energies over the entire bond expected in the system under study by the subsequent relation:

$$CE = \sum C_i D_i / 100 \quad (24)$$

where Ci and Di are the number of expected chemical bonds and the energy of each corresponding bond. The results of CE are listed in table (5). It should be known that the approach of the chemical bond neglects the weakly bonds like dangling bond, other valence defects and van der Walls interactions.

The average heat of atomization H_s

The average heat of atomization Hs is defined as the average bond strength and considered as a direct measure of cohesive energy. For a compound AxByCz, it can be calculated, in kcal/g/atom as the relation [46].

$$H_s = \frac{xH_s^A + yH_s^B + zH_s^C}{x + y + z} \quad (25)$$

where H_s^A, H_s^B, H_s^C are the heat of atomization of the involved elements (Se, S, Sb) as shown table (4) and *x, y, z* are the ratios of these elements in the chalcogenide glass system, respectively. The values of H_s for the Se-S-Sb glass are shown in table (5),These results may due to that the decreasing of the relative atomic mass of chalcogen (Se) or its proportion in a given chalcogenide glass system, increases the average bond strength [47, 48].

The average single bond strength

The average single bond energy H_s/CN , which describe the bond strength (where H_s is the average heat of atomization and *CN* is the average coordination numbers), was calculated and listed in table (5). It was clear that the average single bond energy; H_s/CN, shows a decrease with increasing the Sb content within the glassy composition, while the average heat of atomization and the average coordination number increase, that may consider one of the reasons behind the decrease of the energy gap. This manner of the decrease of H_s/CN; the average single bond energy while the average heat of atomization H_s and the average coordination number C*N* increase, have been noticed recently by E. r. Shaaban et al [49] in the Se-Te-Sb glassy alloys.

Table.1a Values of λ, TM and Tm for amorphous $Se_{80}S_{20}$ thin films corresponding to transmission spectra of the calculated values of refractive index and film thickness are based on the envelope method.

d(nm)	λ_e nm	T_M	T_m	S	n_1	d_1 (nm)	m_o	m	$d_{2(nm)}$	n_2
x=0	568	0.7365	0.5063	1.419	2.48	--	6.52	--	--	2.51
	604	0.7545	0.5195	1.422	2.47	759.7	6.09	6	733.54	2.46
	648	0.7728	0.5354	1.425	2.44	756.9	5.61	5.5	729.91	2.42
	700	0.7861	0.5518	1.427	2.40	772.1	5.11	5	728.52	2.37
	762	0.7988	0.5672	1.430	2.36	771.52	4.62	4.5	724.16	2.33
	842	0.8168	0.5828	1.432	2.34	729.52	4.14	4	718.36	2.29
	944	0.8342	0.5981	1.433	2.32	706.84	3.66	3.5	711.68	2.26
	1088	0.8446	0.6137	1.433	2.28	718.43	3.12	3	714.72	2.22
	1282	0.8532	0.6278	1.429	2.24	--	2.60	2.5	713.64	2.19
	1582	0.865	0.6392	1.419	2.21	--	2.09	2	712.88	2.16

$$\overline{d_1} = 745.9 \text{ nm} \quad \sigma_1 = 24.14\ (3.2\%)$$

$$\overline{d_2} = 720.8 \text{ nm} \quad \sigma_2 = 7.861\ (1.09\%)$$

Table.1b Values of λ, TM and Tm for amorphous $Se_{77.5}S_{20}Sb_{2.5}$ thin films

x	Refractive index $n = a + \frac{b}{\lambda^2}$	
	a	**b** (nm)²
0	**2.117**	**127929.7**
2.5	**2.144**	**139823.9**
5	**2.189**	**142727.6**
7.5	**2.217**	**151876.2**
10	**2.233**	**156016.1**

corresponding to transmission spectra of the calculated values of refractive index and film thickness are based on the envelope method.

d(nm)	λ_e nm	T_M	T_m	S	n_1	d_1 (nm)	m_o	m	$d_{2(nm)}$	n_2
x=2.5	580	0.7248	0.491	1.420	2.53	--	6.52	--	--	2.55
	618	0.7424	0.504	1.423	2.51	783.71	6.06	6	736.75	2.50
	660	0.7584	0.519	1.425	2.48	748.99	5.61	5.5	730.58	2.46
	712	0.7731	0.5355	1.428	2.44	751.32	5.11	5	728.02	2.41
	778	0.7872	0.5514	1.430	2.40	752.33	4.61	4.5	726.61	2.37
	858	0.7996	0.5663	1.432	2.37	731.29	4.12	4	722.42	2.33
	964	0.8117	0.5805	1.433	2.34	721.01	3.62	3.5	719.58	2.29
	1110	0.824	0.5945	1.432	2.31	728.30	3.10	3	719.52	2.25
	1312	0.8362	0.6086	1.428	2.28	--	2.59	2.5	719.01	2.22
	1612	0.8499	0.6208	1.418	2.25	--	2.08	2	715.20	2.19

$$\overline{d_1} = 745.28 \text{ nm} \quad \sigma_1 = 19.45\ (2.6\%)$$

$$\overline{d_2} = 724.19 \text{ nm} \quad \sigma_2 = 6.437\ (0.88\%)$$

Table.1c Values of λ, TM and Tm for amorphous $Se_{75}S_{20}Sb_5$ thin films corresponding to transmission spectra of the calculated values of refractive index and film thickness are based on the envelope method.

d(nm)	λ_e nm	T_M	T_m	S	n_1	d_1 (nm)	m_o	m	$d_{2(nm)}$	n_2
x=5	592	0.7091	0.479	1.422	2.57	--	6.53	--	--	2.59
	628	0.7248	0.499	1.425	2.54	796.47	6.09	6	739.65	2.55
	672	0.7422	0.5053	1.428	2.51	794.99	5.62	5.5	734.75	2.50
	726	0.7586	0.5193	1.431	2.48	751.08	5.15	5	729.24	2.46
	790	0.7739	0.5337	1.433	2.45	731.14	4.68	4.5	722.59	2.41
	878	0.7893	0.5498	1.436	2.42	742.23	4.15	4	723.98	2.37
	984	0.8028	0.5652	1.437	2.39	723.85	3.65	3.5	720.18	2.33
	1128	0.8156	0.5804	1.437	2.35	723.32	3.14	3	718.09	2.30
	1336	0.8278	0.5944	1.434	2.32	--	2.61	2.5	718.72	2.26
	1646	0.839	0.6048	1.428	2.30	--	2.10	2	715.50	2.24

$$\overline{d_1} = 751.87 \text{ nm} \quad \sigma_1 = 29.20\ (3.88\%)$$

$$\overline{d_2} = 724.74 \text{ nm} \quad \sigma_2 = 7.707\ (1.06\%)$$

Table.1d Values of λ, TM and Tm for amorphous $Se_{72.5}S_{20}Sb_{7.5}$ thin films corresponding to transmission spectra of the calculated values of refractive index and film thickness are based on the envelope method.

d(nm)	λ_e nm	T_M	T_m	S	n_1	d_1 (nm)	m_o	m	$d_{2(nm)}$	n_2
x=7.5	600	0.6999	0.4660	1.423	2.61	--	6.49	--	--	2.63
	638	0.7154	0.4796	1.426	2.60	760.34	6.08	6	735.98	2.59
	684	0.7312	0.4940	1.428	2.56	771.70	5.59	5.5	733.49	2.54
	736	0.7460	0.5076	1.431	2.51	767.84	5.10	5	731.30	2.49
	802	0.7612	0.5216	1.434	2.48	744.81	4.63	4.5	725.51	2.45
	888	0.7766	0.5362	1.436	2.45	734.74	4.13	4	722.70	2.40
	998	0.7912	0.5512	1.437	2.42	725.47	3.62	3.5	720.17	2.36
	1146	0.8046	0.5659	1.437	2.39	722.73	3.11	3	718.77	2.33
	1354	0.8169	0.5800	1.434	2.35	--	2.60	2.5	718.08	2.29
	1668	0.8272	0.5915	1.428	2.32	--	2.08	2	716.81	2.27

$$\overline{d_1} = 746.80 \text{ nm} \quad \sigma_1 = 18.63\ (2.49\%)$$

$$\overline{d_2} = 724.76 \text{ nm} \quad \sigma_2 = 6.78\ (0.936\%)$$

Table.1e Values of λ, TM and Tm for amorphous $Se_{70}S_{20}Sb_{10}$ thin films corresponding to transmission spectra of the calculated values of refractive index and film thickness are based on the envelope method.

d(nm)	λ_e nm	T_M	T_m	S	n_1	d_1 (nm)	m_o	m	$d_{2(nm)}$	n_2
x=10	608	0.6915	0.4555	1.423	2.64	--	6.56	--	--	2.65
	646	0.7062	0.4676	1.426	2.61	745.16	6.11	6	739.84	2.60
	692	0.7209	0.4842	1.429	2.57	784.08	5.60	5.5	740.13	2.55
	746	0.7358	0.5012	1.431	2.52	783.84	5.10	5	738.79	2.51
	812	0.7507	0.5141	1.434	2.49	764.68	4.63	4.5	731.03	2.47
	902	0.7667	0.5271	1.436	2.47	751.83	4.13	4	728.32	2.42
	1010	0.7808	0.5407	1.437	2.44	723.52	3.65	3.5	721.95	2.38
	1160	0.7933	0.5548	1.437	2.41	722.84	3.13	3	720.81	2.34
	1372	0.8046	0.5685	1.433	2.37	--	2.61	2.5	721.32	2.31
	1690	0.8149	0.5797	1.427	2.34	--	2.09	2	719.80	2.28

$$\overline{d_1} = 753.71 \text{ nm} \quad \sigma_1 = 23.57\ (3.12\%)$$

$$\overline{d_2} = 729.11 \text{ nm} \quad \sigma_2 = 8.17\ (1.1\%)$$

Table.2 Values of the Cauchy coefficient parameters (a, b) for different composition of amorphous $Se_{80-x}S_{20}Sb_x$ (x=0,2.5,5,7.5,10) thin films.

Table.3 Values of optical energy gap E_g^{opt}, , the single oscillator energy E_o, the dispersion energy parameter E_d, the linear refractive index n_o, high frequency dielectric constant ε_1 and the ratio of concentration carriers to electron effective mass N/m for different composition of amorphous $Se_{80-x}S_{20}Sb_x$ (x=0,2.5,5,7.5,10) thin films.*

	Dispersion parameters					Optical parameters	
x	E_o (eV)	E_d (eV)	$n(o)$	ε_1	$N/m^* \times 10^{56}$ $m^{-3}\,kg^{-1}$	E_g[indir] (eV)	E_e (eV)
0	4.0960 3	15.25	2.17	4.93	2.044	2.66	0.066
2.5	4.0193 9	15.53	2.20	5.08	2.206	2.61	0.070
5	3.9063 8	15.90	2.25	5.29	2.215	2.59	0.071
7.5	3.8410 8	16.18	2.28	5.45	2.325	2.54	0.074
10	3.8109 5	16.34	2.30	5.53	2.325	2.50	0.082

Table.4 Values of density, coordination number, atomic radius, electronegativity, bond energy, heat of atomization for Se, S and Sb.

Property	Se	S	Sb
Density (g/cc)	4.79	2.07	6.62
Coordination number	2	2	3
Atomic radius (Å)	1.22	1.09	1.53
Electronegativity	2.55	2.85	2.05
Bond energy (Kcal mol-1)	44.04	63.34	30.22
Heat of atomization (kcal/g/atom)	49.4	66.68	62

Table.5 Calculated the values of average coordination number (Nc), lone-pair electrons (L and V), the cohesive energy (CE), The average heat of atomization (Hs) and the average single bond energy (Hs/CN).

Sb at. %	N_c	L	Hs (Kcal/g.mol)	Hs/Nc (kcal/g/atom)	CE	Excess of Se-Se bonds
0	2	4	52.856	26.428	2.062	120
2.5	2.025	3.95	53.171	26.257	2.086	107.5
5	2.05	3.9	53.486	26.091	2.109	95
7.5	2.075	3.85	53.801	25.928	2.133	82.5
10	2.1	3.8	54.116	25.77	2.157	70

4 Conclusion

XRD patterns of thermally evaporated $Se_{80-x}S_{20}Sb_x$ (x = 0, 2.5, 5, 7.5, 10) films confirm the amorphous nature and the approximately single phase for all the samples. The optical band gap of the studied films decreases slightly with increasing Sb content, science the value of E_g decreases from 2.66 to 2.5 eV. This decrease in optical band gap may be correlated to the increase of the localized states within the band gap, which refer to the values of Urbach energy. The values of the refractive index increase with the increase of the Sb content within the specimens under investigation. This result may be related to the increased polarizability of the larger Sb atomic radius 1.53 A^0 compared with the Se atomic radius 1.22 A^0. Each of the extinction coefficient and the real, and imaginary parts of the dielectric constant for all the investigated films decrease with increasing the wavelength of incident photons but increase with increasing Sb content. The energy loss factor, VELF and SELF were found to increase with increasing photon energy, taking higher values at the same photon energy for the more Sb concentrations samples. The optical conductivity increases exponentially with increasing photon energy, due to increase in refractive index and absorption coefficient taking higher values at the same photon energy for the specimens, which contain a higher concentration of Sb. On the other side, the electrical conductivity is inversely proportional to photon energy taking slightly higher values for the more Sb content samples. The dispersion parameters such as E_d, ε_1, n_o and N/m^* increase with increasing Sb content while E_0 decreases, which refereeing to the effects of the addition of a metallic element to the covalent chalcogen composition leading to the reduce of energy gab and the increase of the free carrier density, that affect directly on all the dispersion parameters. Non-linear refractive index n_2 was estimated according to two models Tichy- Ticha and Fourier-Snitzer. The two models confirm that the non-linear refractive index decreases with increasing wavelength and increases with increasing Sb content for all the samples under investigation. The structural parameters like cohesive energies, average heat of atomization and number of lone pairs electrons have been estimated, their results refer to that the more stable samples are the more Sb containing samples, but the values of the single bond strength H_s/CN decrease with increasing Sb content refereeing to the decrease of energy gab with increasing Sb content.

Acknowledgment

The authors are grateful to Al-Azhar University for supporting with some of experimental measurements. In addition, the authors thank the Deanship of Scientific Research at King Khalid University (KKU) for funding this research project, Number: (R.G.P2./22/40) under research center for advanced material science.

References

[1] C. Marchand, Characterization of chalcogenide glasses. 1998.Miner., 83(1998), pp.865-871. (12): p.2840-2843.

[2] S. Kumar, M.A.M. Khan, Optical properties of amorphous Se94Te6and Se91Te9thin films deposited by thermal evaporation, Chalcogenide Lett. 9 (2012)145–149.

[3] M. Popescu, Disordered chalcogenide optoelectronic materials: phenomena and applications, J. Optoelectronic. Adv. Mater. 7 (2005) 2189–2210.

[4] D. Aggarwal, J.S. Sanghera, Development and applications of chalcogenide glass optical fibers at NRL, J. Optoelectronic. Adv. Mater. 4 (2002) 665–678.

[5] A. Goel, E.R Shaaban, D.U. Tulyaganov, J.M.F.Ferreira, " Study of crystallization kinetics in glasses along the diopside-Ca- Tschermak join"Journal of the American Ceramic Society 91(2008) 2690-2697.

[6] Quinn RK, Johnson RT. Journal of Non-crystalline Solids 1979;7:53.

[7] Vazquez J, Wagner C, Villares P. Journal of Non-crystalline Solids 1998;235:548.

[8] Y. Yu, R.H. Wang, Q. Chen, L. Peng, High-Quality Ultralong Sb2Se3 and Sb2S3 Nanoribbons on a Large Scale via a Simple Chemical Route, J. Phys. Chem. B 110(2006) 13415.

[9] Park JH, Jeong JH, Choi DJ. Study on the crystallization behavior of nitrogen-doped Sb Se films for PCRAM applications. Phys Status Solidi A 2016; 213:1526-34.

[10] ElS. Yousef, A. El-Adawy, N. El Koshkhany, E.R. Shaaban, Optical and acoustic properties of TeO2/WO3 glasses with small amount of additive ZrO2, Journal of Physics and Chemistry of Solids 67 (2006) 1649.

[11] Wang M, Wu W, Zheng X, Hou X, Liu C, Hao Q, et al. Preparation of uniform Sb2Se3 nanorods by hot-injection polyol process and their application in photodetector. Mater Lett 2017; 193:191–4.

[12] Lai Y, Chen Z, Han C, Jiang L, Liu F, Li J, et al. Preparation and characterization of Sb2Se3 thin films by electro deposition and annealing treatment. Appl Surf Sci 2012; 261:510–4.

[13] C. Ghosh, B.P. Varma, Optical properties of amorphous and crystalline Sb2S3 thin films, Thin Solid Films 60 (1979) 61.

[14] J. Grigas, J. Meshkauskas, A. Orliukas, A Dielectric properties of Sb2S3 at microwave frequencies. 1976.37(1): p.k39-k41.

[15] X. Wang, J. Li, W. Liu, S. Yang, C. Zhu, T. Chen, A fast chemical approach towards Sb2S3 film with a large grain size for high-performance planar heterojunction solar cells, Nanoscale 9 (10) (2017) 3386–3390.

[16] Y.C. Choi, Y.H. Lee, S.H. Im, J.H. Noh, T.N. Mandal, W.S. Yang, S.I. Seok, Efficient inorganic-organic heterojunction solar cells employing Sb2(Sx/Se1−x)3 graded composition sensitizers, Adv. Energy Mater. 4 (7) (2014) 1301680.

[17] B. Yang, S. Qin, D. Xue, C. Chen, Y. He, D. Niu, H. Huang, J. Tang, in situ sulfurization to generate Sb2(Se1−xSx)3 alloyed films and their application for photovoltaics, Prog. Photovolt.: Res. Appl. 25 (1) (2017) 113–122.

[18] W. Qiua, C. Zhanga, S. Chenga, Q. Zhenga, X. Yua, H. Jiaa, B. Wuc, The crystal structure, electronic structure and photoelectric properties of a novel solar cells absorber material Sb2Se3−xSx, Solid State Chemistry. 271 (2019) 339–345.

[19] Ramakanta Naik, R. Ganesan, The effect of compositional variations on the optical properties of SbxSe60-x S40 thin films, Thin Solid Films. 579 (2015) 95–102.

[20] J.C. Manifacier, J. Gasiot, J.P. Fillard, J. Phys. E. 9 (1976) 1002.

[21] F.A. Jenkins, H.E. White, Fundamentals of Optics, McGrow-Hill, New York, 1957.

[22] S. H. Wemple and W. DiDomenico, Phys. Rev. B3 (1971) 1338.

[23] K. Tanaka,Thin Solid Films 66(1980) 271.

[24] M. Krbal, T. Wagner, Mil. Vlcek, Mir. Vlcek, M. Frumar, J. Non-Cryst. Solids 352 (2006) 2662.

[25] N. Mott, E. Davis, R. Street, States in the gap and recombination in amorphous semiconductors, Philosophical Magazine, 32 (1975) 961.

[26] R. Valalova, L. Tichy, M. Vlcek, H. Ticha, Phys. Status Solidi a 181(2000)199.

[27] J. Tauc, In amorphous and liquid semiconductors, Ed. J. Tauc, Plenum Press New York, (1974) 171.

[28] F .Urbach,Phys. Rev. B 92 (1953)1324.

[29] E. A. Davis and N. F. Mott,Phil. Mag. 22 (1970) 903

[30] N.A .Bakr, A. Funde, V. Waman, M. Kamble, R. Hawaldar, D. Amalnerkar, S. Gosavi, S. Jadkar, Determination of the optical parameters of a-Si: H thin films deposited by hot wire–chemical vapour deposition technique using transmission spectrum only, Pramana, 76 (2011) 519.

[31] E.R. Shaaban, I. Kansal, S. Mohamed, J.M. Ferreira, Microstructural parameters and optical constants of ZnTe thin films with various thicknesses, Physica B: Condensed matter, 404 (2009) 3571-3576.

[32] El-Nahass MM, Ali MH, El-denglawey A. Structural and optical properties of nano spin coated sol−gel porous TiO2 films. Trans. Nonferr. Met. Soc. China.2012;22:3003–12011.

[33] Park WD. Optical constants and dispersion parameters of CdS thin film prepared bychemical bath deposition. Trans Elect Electron Mater 2012; 13:196–9.

[34] J.I. Pankove, Optical Processes in Semiconductors, Courier Corporation, New York, 1975.

[35] F. Yakuphanoglu, A. Cukurovali, I. Yilmaz, Refractive index and optical absorption properties of the complexes of a cyclobutane containing thiazolyl hydrazone ligand, Optical Materials, 27 (2005) 1363.

[36] H. Ticha, L. Tichy, Semiempirical relation between non-linear susceptibility (refractive index), linear refractive index and optical gap and its application to amorphous chalcogenides, Journal of Optoelectronics and Advanced Materials, 4 (2002) 381.

[37] C.C. Wang, Empirical relation between the linear and the third-order nonlinear optical susceptibilities, Physical Review B, 2 (1970) 2045.

[38] E.R. Shaaban, M.M. Mahasen, M.M. Soraya, E.S. Yousef, S.A. Mahmoud, G.A.M. Ali, H.A. Elshaikh, Dilute magnetic semiconductor of ZnCoSe thin films: Structural, optical and magnetic characteristics, Journal of the American Ceramic Society, (2018) doi.org/10.1111/jace.16260.

[39] J. Fournier, E. Snitzer, The nonlinear refractive index of glass, IEEE Journal of Quantum Electronics, 10 (1974) 473.

[40] M. Asobe, T. Kanamori, K.i. Kubodera, Applications of highly nonlinear chalcogenide glass fibers in ultrafast all-optical switches, IEEE Journal of Quantum Electronics, 29 (1993) 2325.

[41] T. Töpfer, J. Hein, J. Philipps, D. Ehrt, R. Sauerbrey, Tailoring the nonlinear refractive index of fluoride-phosphate glasses for laser applications, Applied Physics B, 71 (2000) 203.

[42] A. F. Loffe and A. R. Regel, Prog. Semicond. 4 (1960) 239

[43] M. El-Hagary, M. Emam-Ismail, E. Shaaban, A. Al-Rashidi, S. Althoyaib, Composition, annealing and thickness dependence of structural and optical studies on Zn1− xMnxS nanocrystalline semiconductor thin films, Materials Chemistry and Physics, 132 (2012) 581-590.

[44] E. R. Shaaban, I. B. I. Tomsah, J. Therm. Anal. Calorim.105 (2011) 191.

[45] W. H. Zachariasen, J. Am. Chem. Soc. 54 (1932) 3841.

[46] V. Sadgopam and H. C. Gotos, On the relationship of semiconductors compounds properties and the average heat of atomization, Solid State Electron. 8(1965) 529.

[47] E. Mytilineou, Chalcogenide amorphous semiconductors: chemical modification or dopind, J. of Opto.andAdv.Mat. 4 (2002) 705.

[48] Y. Kawamoto, S. Tsuchihashi, J. Cream Assoc. Japan. 77 (1969) 12.

[49] E. R. Shaaban, H. A. Elshaikh, M. M. Soraya, Optoelectronics and Advanced Materials- Rapid Communications 9 (2015) 587-600.